



## Note

Algae 2021, 36(4): 241-261  
<https://doi.org/10.4490/algae.2021.36.8.27>

Open Access



# *Amphidinium stirisquamatum* sp. nov. (Dinophyceae), a new marine sand-dwelling dinoflagellate with a novel type of body scale

Zhaohe Luo<sup>1,\*</sup>, Na Wang<sup>1</sup>, Hala F. Mohamed<sup>1,2</sup>, Ye Liang<sup>3</sup>, Lulu Pei<sup>1,4</sup>, Shuhong Huang<sup>1</sup> and Haifeng Gu<sup>1</sup>

<sup>1</sup>Third Institute of Oceanography, Ministry of Natural Resources, Xiamen 361005, China

<sup>2</sup>Botany & Microbiology Department, Faculty of Science, Al-Azhar University (Girls Branch), Cairo 11751, Egypt

<sup>3</sup>School of Marine Sciences, Nanjing University of Information Science and Technology, Nanjing 210044, China

<sup>4</sup>Technical Innovation Service Platform for High Value and High Quality Utilization of Marine Organism, Fuzhou University, Fuzhou 350108, China

*Amphidinium* species are amongst the most abundant benthic dinoflagellates in marine intertidal sandy ecosystems. Some of them produce a variety of bioactive compounds that have both harmful effects and pharmaceutical potential. In this study, *Amphidinium* cells were isolated from intertidal sand collected from the East China Sea. The two strains established were subjected to detailed examination by light, and scanning and transmission electron microscopy. The vegetative cells had a minute, irregular, and triangular-shaped epicone deflected to the left, thus fitting the description of *Amphidinium sensu stricto*. These strains are distinguished from other *Amphidinium* species by combination characteristics: (1) longitudinal flagellum inserted in the lower third of the cell; (2) icicle-shaped scales,  $276 \pm 17$  nm in length, on the cell body surface; (3) asymmetrical hypocone with the left side longer than the right; and (4) presence of immotile cells. Therefore, they are described here as *Amphidinium stirisquamatum* sp. nov. The molecular tree inferred from small subunit rRNA, large subunit rRNA, and internal transcribed spacer-5.8S sequences revealed that *A. stirisquamatum* is grouped together with the type species of *Amphidinium*, *A. operculatum*, in a fully supported clade, but is distantly related to other *Amphidinium* species bearing body scale. Live *A. stirisquamatum* cells greatly affected the survival of rotifers and brine shrimp, their primary grazers, making them more susceptible to predation by the higher tropic level consumers in the food web. This will increase the risk of introducing toxicity, and consequently, the bioaccumulation of toxins through marine food webs.

**Key Words:** benthic-epiphytic dinoflagellate; food chain; harmful algae; phylogeny; toxin

## INTRODUCTION

Benthic microalgae are an important source of primary organic supplements in shallow coastal environments (Forster et al. 2016). Since resuspended microphytobenthic communities are often more abundant than exclusively phytoplankton communities in tidal flat eco-

systems, it is hypothesized that benthic microalgae may support both benthic and pelagic food webs in intertidal and adjacent subtidal areas (De Jonge and Van Beuselom 1992, Lucas et al. 2000, Facca et al. 2002). Therefore, significant attention has been paid to the role of microphy-



This is an Open Access article distributed under the terms of the Creative Commons Attribution Non-Commercial License (<http://creativecommons.org/licenses/by-nc/3.0/>) which permits unrestricted non-commercial use, distribution, and reproduction in any medium, provided the original work is properly cited.

Received April 14, 2021, Accepted August 27, 2021

\*Corresponding Author

E-mail: [luozhaohe@tio.org.cn](mailto:luozhaohe@tio.org.cn)

Tel: +86-158-60728830, Fax: +86-592-2195157

tobenthic communities in coastal ecosystem food webs (De Jonge and Van Beuselom 1992).

The genus *Amphidinium* Claparède & Lachmann represents one of the most abundant members of benthic dinoflagellates in marine intertidal and neritic sandy ecosystems (Dodge and Hart-Jones 1982, Murray and Patterson 2002). Some species have received a significant amount of scientific attention due to the increased occurrence of benthic harmful algal blooms in coastal zones worldwide (Berdal et al. 2017, Gárate-Lizárraga et al. 2019, Tester et al. 2020). Also, some *Amphidinium* spp. can produce ichthyotoxins that have adverse effects on marine ecosystems and public health (Kobayashi et al. 1991, Huang et al. 2009, Murray et al. 2015). *Amphidinium* was traditionally defined by its small epicone size (Claparède and Lachmann 1859). Approximately 200 morphologically dissimilar marine and freshwater *Amphidinium* species have been established (Daugbjerg et al. 2000, Saldarriaga et al. 2001, Guiry and Guiry 2021). However, molecular studies have revealed that the genus *Amphidinium* is a heterogeneous assemblage (Saldarriaga et al. 2001). And many species originally considered as members of the genus *Amphidinium* subsequently have been reclassified as belonging to new genera, like *Ankistrodinium* Hoppenrath, Murray, Sparmann & Leander, *Apicoporus* Sparmann, Leander & Hoppenrath, *Prosoaulax* Calado & Moestrup, *Togula* Flø Jørgensen, Murray & Daugbjerg, *Testudodinium* Horiguchi, Tamura, Katsumata & A. Yamaguchi and so on (Jørgensen et al. 2004a, Calado and Moestrup 2005, Sparmann et al. 2008, Hoppenrath et al. 2012, Horiguchi et al. 2012). A recent emendation of the genus definition was performed after reinvestigation of *A. operculatum* Claparède & Lachmann, the type species, and putative relatives of *Amphidinium* (Jørgensen et al. 2004b, Murray et al. 2004). The genus of *Amphidinium sensu stricto* now only includes those athecate benthic or endosymbiotic dinoflagellates with minute irregular triangular- or crescent-shaped epicones that are deflected towards the left (Jørgensen et al. 2004b). Twenty-three species have been checked and assigned to *Amphidinium sensu stricto* so far (Jørgensen et al. 2004b, Murray et al. 2004, Dolapsakis and Economou-Amilli 2009, Karafas et al. 2017). The rest of species that do not fit the criteria for the redefined genus, but have not yet been investigated to determine the generic affinities, are classified as *Amphidinium sensu lato* (Hoppenrath et al. 2014, Guiry and Guiry 2021).

Different morphological features have been used to identify *Amphidinium sensu stricto* species, such as cell size and shape, location of longitudinal flagellum, life

cycle stage, and body scales morphology (Claparède and Lachmann 1859, Maranda and Shimizu 1996, Sekida et al. 2003). However, there are no unambiguous features that can be used to differentiate *Amphidinium sensu stricto* species, and some characteristics can even overlap among species (Murray and Patterson 2002, Jørgensen et al. 2004b, Murray et al. 2004). Body scale possess or not as well as the morphology of it is a useful diagnostic characterization. To date, two types of body scales have been recorded among *Amphidinium sensu stricto* species. The first, round doughnut-like body scale on the cell surface, were reported in *A. massartii* Biecheler (*A. massartii* and *A. cf. massartii*) (Sekida et al. 2003, Murray et al. 2012). Recently, these scales have been also recorded on the cell surface of *A. paucianulatum* Karafas & Tomas and *A. theodori* Tomas & Karafas (Karafas et al. 2017) making it non-unique. The second type of scale, distinct cup-shaped with three-dimensionality, were only recorded on *A. cupulatisquama* M. Tamura & T. Horiguchi cell surfaces (Tamura et al. 2009). Additional types of body scales could be expected with more detailed morphological investigation of both *Amphidinium sensu stricto* and the large number of *Amphidinium sensu lato* species. The location of longitudinal flagellum is also considered an important diagnostic characterization (Jørgensen et al. 2004b, Murray et al. 2004, Karafas et al. 2017). Three groups within *Amphidinium sensu stricto*, which show consistency with regards to their lower, anterior, and middle third of the cell positioning of longitudinal flagellum insertion, have been identified. However, such division was not supported by rRNA-based phylogeny, and the relationship among different groups still need to be determined (Murray et al. 2004, Karafas et al. 2017). In brief, a combination of characteristics seems to be the best approach to differentiate *Amphidinium* species (Karafas et al. 2017).

Polyketides, such as amphidinol analogs, are the main toxic secondary metabolite of *A. klebsii* Kofoid & Swezy and *A. carterae* Hulbert, and have been widely reported (Echigoya et al. 2005, Inuzuka et al. 2014, Nuzzo et al. 2014, Wellkamp et al. 2020). Almost all investigated amphidinols have been tested for a variety of biological activities, and antifungal and hemolytic effects were observed (Echigoya et al. 2005, Inuzuka et al. 2014, Nuzzo et al. 2014). In addition, Amphidinol 22 and Lingshuol exhibited cytotoxic and anticancerous properties against some cell lines (Huang et al. 2004a, 2004b, Martínez et al. 2019). The negative effects of *Amphidinium* cells on filter-feeding zooplankton, shellfish, and fish have not been fully investigated. The glycoglycerolipid extracted

from *A. carterae* was found to be toxic to pearl oysters (Wu et al. 2005). A gill-damaging toxin in fish has been recorded in a bloom of *A. carterae* in a coastal lagoon in Sydney, Australia (Murray et al. 2015).

Morphology-based recording of *Amphidinium sensu stricto* along the Chinese coast is rare, and only four species, i.e., *A. carterae*, *A. massartii*, *A. gibbosum* (Maranda & Shimizu) Flø Jørgensen & Murray, and *A. operculatum* have been reported (Wu et al. 2005, Zhang 2015). The toluene extract of cultured *A. carterae* isolated from Sanya, Hainan Island was found to be toxic to pearl oysters (Wu et al. 2005), indicating the potential risk of *Amphidinium* spp. to mudflat aquaculture. In this respect, our knowledge of *Amphidinium* in coastal ecosystem food webs remains limited, and identification of a greater number of *Amphidinium* species on the Chinese coast can be expected. In this study, we collected samples from beach sand from the East China Sea and isolated single cells in order to establish strains of *Amphidinium sensu stricto*. Two strains were established, and their morphology was examined carefully in detail using light, and scanning and transmission electron microscopy. In addition, the molecular phylogeny was inferred based on small sub-unit (SSU) rRNA, large subunit (LSU) rRNA, and internal transcribed spacer (ITS)-5.8S rRNA sequences. The toxicity impact of the new *Amphidinium* on brine shrimp (*Artemia salina* Linnaeus) and rotifer (*Brachionus plicatilis* Müller) survival was evaluated.

## MATERIALS AND METHODS

### Specimen collection and cultivation

Wet beach sand was collected from the East China Sea. *Amphidinium stirisquamatum* strain TIO971 was isolated from Xishawan beach park ( $24^{\circ}52'56.41''$  N,  $118^{\circ}54'58.89''$  E), Fujian province on Apr 18, 2019, while strain TIO955 was collected from Pingtan ( $25^{\circ}26'33.85''$  N,  $119^{\circ}46'58.89''$  E), Fujian province on Apr 16, 2019. The upper centimeter of sand was collected from the seabed, and deposited into a 50 mL plastic bottles containing seawater collected at the same location, and brought back to laboratory. Each sample was transferred into a 1 L polycarbonate bottle with filtered seawater, and stirred vigorously to detach the epibenthic cells. The suspension materials were afterward filtered through 120 µm and 10 µm filters, and the 10–120 µm materials were rinsed with 0.22 µm-filtered seawater. Single cells were isolated from this fraction with a pipette tip under an Eclipse TS100 inverted

microscope (Nikon, Tokyo, Japan) into a 96-well culture plate full of f/2-Si medium (Guillard and Ryther 1962). The plate was positioned at  $25^{\circ}\text{C}$ ,  $90 \mu\text{mol photons m}^{-2} \text{s}^{-1}$  cool-white light, and under a light : dark cycle of 12 : 12 h (standard culture conditions). The clonal cultures were transferred to 50 mL polystyrene tissue culture flasks, and maintained under the standard culture conditions.

### Light microscopy

Living cells were observed and photographed using a Zeiss AX10 microscope (Carl Zeiss, Göttingen, Germany) equipped with an AxioCam HRc digital camera. Thirty cells of strain TIO971 were measured using Axiovision (4.8.2 version). To observe the location and shape of the nucleus, *Amphidinium* cells were stained with 1 : 100,000 Sybr-Green (Sigma, St. Louis, MO, USA) for 1 min, and photographed under the Zeiss fluorescence microscope equipped with a Zeiss-38 filter cube (excitation 470/40, beam splitter 495, emission 525/50). Chloroplast auto-fluorescence microscopy was photographed on live cells using a Leica DM6000B microscope (Leica, Wetzlar, Germany) equipped with a G filter set (emission 495/15, beam splitter 510, emission 530/30), and carried out using a Leica DFC300 FX camera.

### Scanning electron microscopy

Two different fixatives were processed to prepare for scanning electron microscopy (SEM): (1) mid-exponential batch cultures were fixed overnight at  $4^{\circ}\text{C}$  with 1% OsO<sub>4</sub> prepared with 0.2 µm-filtered seawater; and (2) cultures were fixed for 2 h in 2% glutaraldehyde prepared with 0.2 µm-filtered seawater. The supernatant was removed, and the settled cell pellets were transferred to a coverslip coated with poly-L-lysine (molecular weight 70,000–150,000). Subsequently, the attached cells were rinsed with Milli-Q water for 10 min. Cells were dehydrated through a graded ethanol (i.e., 10, 30, 50, 70, 90 and 3x in 100%) for 10 min every step. The attached cells were then critical point dried in a K850 CPD equipment (Quorum, West Sussex, UK), sputter-coated with platinum, and examined with a Zeiss Sigma FE (Carl Zeiss Inc., Oberkochen, Germany) scanning electron microscope. Images were presented on a black background using Photopea online program (<https://www.photopea.com/>).

### Transmission electron microscopy

Thirty milliliters of logarithmic phase culture were

fixed in 2.5% glutaraldehyde for 3 h at 20°C, concentrated in a Primo R centrifuge (Thermo Scientific, Waltham, MA, USA) at 2,500g for 10 min at 20°C, and rinsed three times with cooled 0.22 µm-filtered seawater for 10 min each. Cells were post-fixed in cold 1% OsO<sub>4</sub> prepared with 0.22 µm-filtered sterile seawater overnight at 4°C. The cells were washed with filtered seawater, 50% filtered seawater and Milli-Q water for 10 min each step. Cells were dehydrated through a graded ethanol (i.e., 10, 30, 50, 70, 90 and 3× in 100%) for 30 min each. The cell pellet was embedded in Spurr's resin (Spurr 1969) and sectioned with a Leica EM UC6 ultramicrotome (Leica, Vienna, Austria), stained with uranyl acetate and lead citrate, and examined with a JEM1400 transmission electron microscope (JEOL, Tokyo, Japan).

### Molecular analysis

Total genomic DNA was extracted from 15 mL of mid-exponential batch cultures using a MiniBEST genomic DNA Extraction Kit (Takara, Tokyo, Japan). PCR amplifications were performed by 1× PCR buffer, 50 µmol dNTP mixture, 0.2 µmol of each primer, 10 ng of genomic DNA, and 1 U of Ex-Taq DNA Polymerase (Takara) in 50 µL reactions. The SSU rRNA gene was amplified using the PRIMER A/PRIMER B primers (Medlin et al. 1988) or SR1c/SR12b (Takano and Horiguchi 2004). The full length ITS1–5.8S–ITS2 was amplified using ITS A/ITS B primers (Adachi et al. 1996). The LSU rRNA gene was amplified using the primers of D1R/28-1483R (Scholin et al. 1994, Daugbjerg et al. 2000). PCR amplification was carried out in a Mastercycler (Eppendorf, Hamburg, Germany) using the thermal programs: 4 min at 94°C, 30 cycles of 50 s at 94°C, 50 s at 47°C, 50 s at 72°C, and a final extension of 10 min at 72°C with. The PCR product was purified and sequenced by Beijing Genomics Institute (BGI, Guangzhou, China).

### Sequence alignment and phylogenetic analyses

The newly obtained SSU rRNA sequences were aligned to a large multiple publicly available complete or nearly complete (>1,500 bp) dinoflagellate SSU rRNA sequences using MAFFT v7.110 (Katoh and Standley 2013) online program (<http://mafft.cbrc.jp/alignment/server/>) with L-INS-I (Carroll et al. 2007). Alignments were manually inspected with BioEdit v7 (Hall 1999). *Syndinium turbo* was used as the outgroup. The package jModelTest 2 (Darriba et al. 2012) was used to choose the most appropriate model of molecular evolution model under Akaike

Information Criterion. Bayesian inference (BI) was carried out using MrBayes 3.2 (Ronquist et al. 2012) with the selected substitution model. Four Markov chain Monte Carlo (MCMC) chains were running for 5,000,000 generations, sampling each 100 generations. Tracer ver. 1.7.1 software package (<http://tree.bio.ed.ac.uk/software/tracer/>) to process MCMC trace convergence diagnostics, and the first 10% of burn-in trees were castoff. In order to examine the posterior probabilities of each tree clade, a majority rule consensus tree was created. Maximum likelihood (ML) analyses were carried out with RaxML v7.2.6 (Stamatakis 2006) on the T-REX online website (Boc et al. 2012) using the GTR + G model. phylogenetic node support was evaluated with 500 bootstrap replicates.

Newly obtained LSU rRNA (D1-D6) sequences and all publicly available *Amphidinium sensu stricto* LSU rRNA sequences incorporated into a representative dinoflagellate taxa LSU rRNA sequences data set (Murray et al. 2005), and aligned using MAFFT v7.110. *Oxyrrhis marina* were used as the outgroup, and the following processing were same as SSU rRNA phylogeny described above. Newly obtained ITS sequences were aligned with all publicly available *Amphidinium sensu stricto* sequences downloaded from the GenBank. *Karlodinium armiger* were used as the outgroup, and the following processing were same as SSU rRNA phylogeny described above.

### Brine shrimp and rotifer toxicity assay

The resting eggs of brine shrimp, *Ar. salina*, were hatched in 6-well plate containing 0.2 µm-filtered seawater (salinity = 30). *B. plicatilis* were maintained in a laboratory and fed with marine *Chlorella* sp. prior to the experiment. *Chlorella* sp. is an optimal food for *B. plicatilis* (Sun et al. 2017), and was used as the control group. Ten newly hatched *Ar. salina* (<2 h old) or ten male neonatal *B. plicatilis* were isolated into each of a 6-well tissue culture plate containing 10 mL of four different culture food combinations: (1) 0.2 µm-filtered seawater as control for *Ar. salina* and *Chlorella* sp. ( $1.0 \times 10^6$  cells mL<sup>-1</sup>) as control for *B. plicatilis*, respectively; (2) *Amphidinium stirisquamum* live culture (TIO971 or TIO955); (3) *Chlorella* sp. ( $1.0 \times 10^6$  cells mL<sup>-1</sup>) + *A. stirisquamum* live culture (TIO971 or TIO955); and (4) liquid nitrogen freeze-thaw treated *A. stirisquamum* culture (TIO971 or TIO955 killed and ruptured cells). Different cell densities (100, 1,000, 2,000, 3,000, 4,000, and 5,000 cells mL<sup>-1</sup>) of *A. stirisquamum* were investigated. Each food treatment was established in three replicates. *Ar. salina* and *B. plicatilis*

were monitored at 24-h intervals under a Zeiss Discovery v.8 inverted microscope (Carl Zeiss Inc.). The numbers of living original individuals were counted, and the dead ones were removed from the wells. Two factor analysis of variance between control and different food treatment groups was conducted using Microsoft Office Excel 2016.

## RESULTS

### *Amphidinium stirisquamum* Z. Luo, Na Wang & H. Gu sp. nov.

**Description.** Cells were ovoid, dorsoventrally flattened, with a slightly pointed antapex, 30–37 µm in length and 24–30 µm in width; the epicone was triangle-shaped, left-deflecting, 8.6 ± 0.8 µm in length; the hypocone was asymmetrical, left side longer than the right; the nucleus was elongated, located in the cell posterior; contained a single yellow-golden chloroplast, radiated from centrally located pyrenoids, and branched peripherally; immotile cells were spherical, 31–34 µm in diameter; body scales were icicle-shaped.

**Habitat.** Marine and sandy sediments.

**Holotype.** A SEM stub from strain TIO971 marked as TIO971-20191014 and deposited at Third Institute of Oceanography, Ministry of Natural Resources, Xiamen 361005, China.

**Type locality.** Xishawan beach park, Fujian, East China Sea (24°52'56.41" N, 118°54'58.89" E).

**Etymology.** Latin *stiria* – icicle-shaped, *squama* – scale (icicle-shaped scale), indicating the shape of body scales.

**GenBank accession number.** MZ668341 (LSU rRNA), MZ663990 (ITS), and MZ663992 (SSU rRNA) of strain TIO955; MZ668342 (LSU rRNA), MZ663991 (ITS), and MZ663993 (SSU rRNA) of strain TIO971.

Cells of the *A. stirisquamum* strain TIO971 were oval and dorsoventrally flattened (Fig. 1A–C, Supplementary Video S1). Cells were 30.3–37.0 µm long (mean ± SD, 34.6 ± 2.0 µm, n = 30) and 24.1–30.2 µm wide (26.9 ± 1.4 µm, n = 30), with the length/width ratio changing from 1.20 to 1.37 (1.29 ± 0.05, n = 30). The epicone was triangular and relatively minute compared to the hypocone, and was left-deflecting, 8.6 ± 0.8 µm long (n = 10) (Fig. 1A & B). The hypocone was asymmetrical, with the left side longer than the right (Fig. 1A–C). The outline of both sides of the hypocone was convex with the broadest width in the cell center (Fig. 1A–C). Many lipid globules were observed in the cell periphery (Fig. 1C). The nucleus was elongated and located at the end of cell posterior (Fig. 1B & D). A

single multilobed chloroplast was yellow-golden, and the lobes radiated from centrally located pyrenoids and branched peripherally (Fig. 1A, B & E). Immotile cells were observed in old cultures of strain TIO971 with a diameter of 31.1–33.6 µm (32.5 ± 0.9 µm, n = 10) (Fig. 1F). Asexual division was by bipartition in the motile cell (Fig. 1G).

Under SEM, the cingulum was displaced and the proximal end was distant from the sulcus (Fig. 2A). The ventral ridge was 13.1 ± 1.1 µm long (n = 10), and connected the two flagella insertion points (Fig. 2A). The longitudinal flagellum was inserted in the lower third of the cell, and at the beginning of the sulcus (Fig. 2A). The sulcus was narrow and shallow, but became wider at the posterior end (Fig. 2A & F). Icicle-shaped body scales were observed on the surface of the cell body but not on the flagella (Fig. 2A–E), when osmium tetroxide was used for fixation. The plasma membrane was smooth with numerous trichocyst pores on the surface (Fig. 2F & G) when the body scales were stripped away by glutaraldehyde fixation.

Under transmission electron microscopy (TEM), a longitudinal section through the cell exhibited a typical large dinokaryon with a spherical nucleolus, as well as multiple condensed chromosomes located at the cell posterior (Fig. 3A–C). Lipid globules were present throughout the cytoplasm (Fig. 3A). An unknown organelle was found behind the dinokaryon and sulcus (Fig. 3B). The lobes of chloroplast radiated from centrally located pyrenoids and branched peripherally (Fig. 3A). The thylakoids were grouped in fives to form lamellae (Fig. 3D). The pyrenoid matrix was traversed by thylakoids (Figs 3A & 4A). The pusule comprised a central chamber and spherical collecting tubes, which radiated from the central chamber nearby the transverse flagellum root (Fig. 4B). Numerous mitochondria with tubular cristae were scattered throughout cytoplasm (Fig. 4C & D). Golgi bodies and trichocysts were present (Fig. 4C & D). Body scales were arranged outside the plasma membrane and covered the entire cell body (Fig. 4D). The body scales were icicle-shaped with a length of 276 ± 17 nm (Fig. 4D).

## Molecular phylogeny

The *A. stirisquamum* strains (TIO955 and TIO971) shared identical SSU rRNA, LSU rRNA, and ITS sequences. The sequences of the closest species to *A. stirisquamum* in phylogenetic trees were compared. From a comparison of SSU rRNA gene sequences, *A. stirisquamum* showed differences from the *A. operculatum* strain TAK-0 and

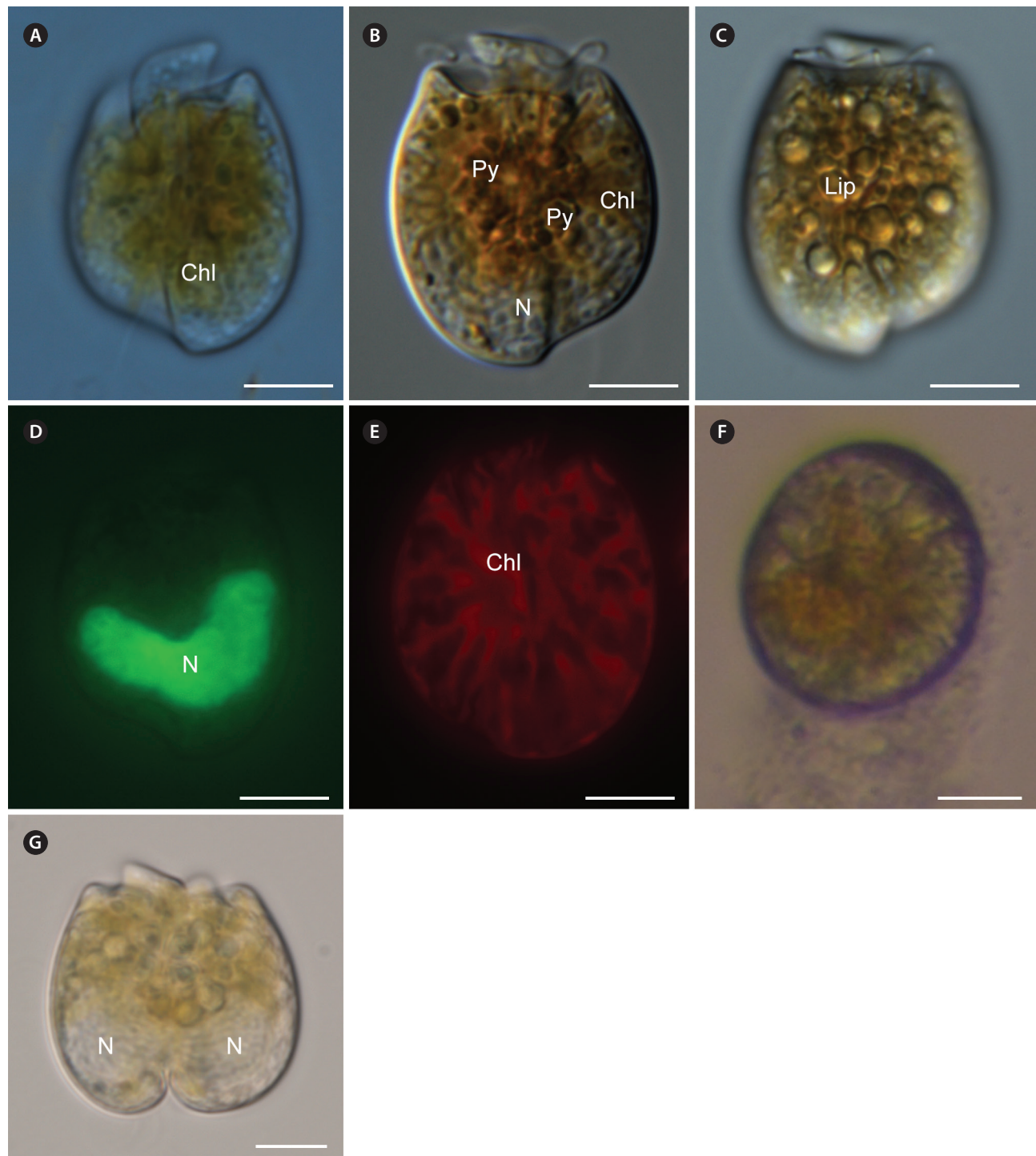


**Fig. 1.** *Amphidinium stirisquamum* sp. nov. light microscopy (LM). (A) Ventral view showing the cell shape and radiated chloroplasts (Chl). (B) Dorsal view showing the centrally located pyrenoids (Py) and radiated chloroplasts (Chl). (C) Dorsal view showing the lipid globules (Lip) in the periphery of cell. (D) Fluorescence LM image of a Sybr-Green stained cell showing the nucleus (N) location and shape. (E) Fluorescence LM image of the ventral view showing reticulate chloroplasts (Chl). (F) Immotile cell. (G) Lateral view showing the dividing cells. Scale bars represent: A–G, 10 µm.

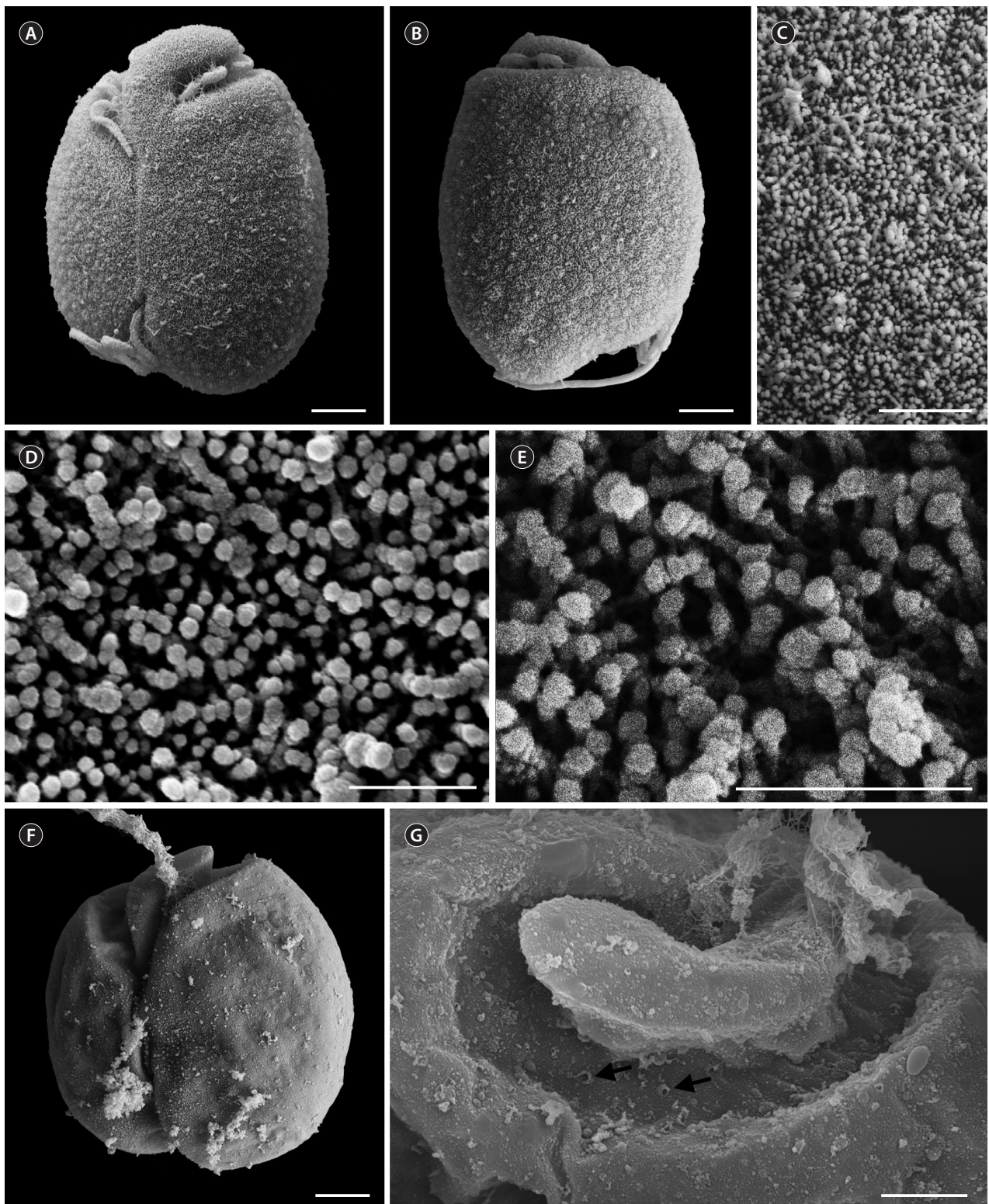


**Fig. 2.** *Amphidinium stirisquamatum* sp. nov. scanning electron microscopy images. (A) Ventral view of an osmium tetroxide fixed cell showing the epicone shape, ventral ridge, points of flagellar insertion and body scales. (B) Dorsal view of an osmium tetroxide fixed cell showing the cell shape and body scales. (C-E) A close-up view in different resolution of icicle-shaped body scales on cell surface. (F) Ventral view of a glutaraldehyde fixed cell showing the cell shape, and smooth plasma membrane. (G) A close-up view of epicone showing the trichocyst pore (arrows) on cell surface. Scale bars represent: A, B & F, 5  $\mu\text{m}$ ; C & G, 2  $\mu\text{m}$ ; D & E, 0.5  $\mu\text{m}$ .

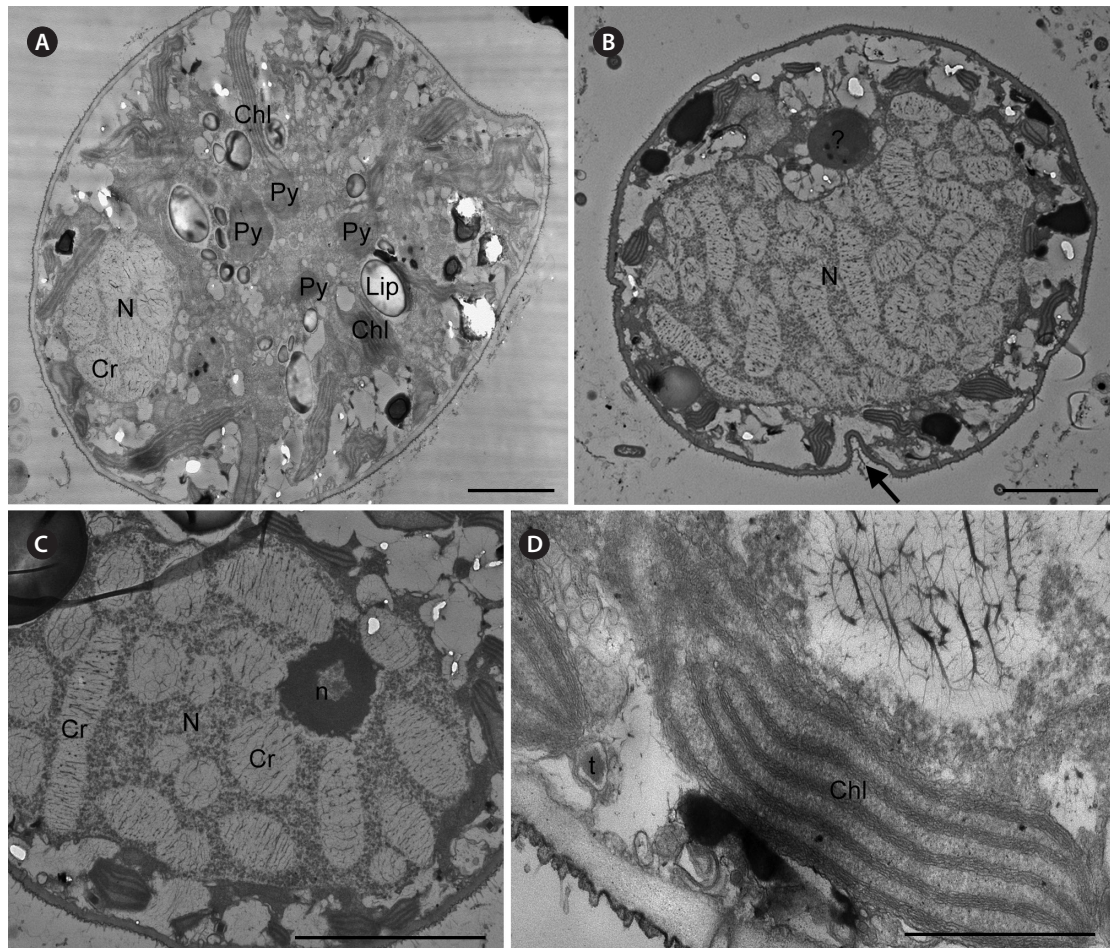


**Fig. 3.** *Amphidinium stirisquamum* sp. nov. transmission electron microscopy images (TEM). (A) Longitudinal section of a cell, showing arrangement of the organelles; the nucleus (N), condensed chromosomes (Cr), pyrenoids (Py), chloroplast (Chl), and lipid globules (Lip). (B) Transverse section of the cell showing nucleus (N), the unknown organelle (?), and the position of sulcus (arrow). (C) Nucleus showing the spherical nucleolus (n) and condensed chromosomes (Cr). (D) Chloroplast (Chl) showing the thylakoids which are grouped in five to form lamellae. Scale bars represent: A–C, 5 µm; D, 1 µm.

*Amphidinium* sp. strain HG213 from Japan in 181 and 321 positions (with 89.0% and 78.6% similarity), respectively. For LSU rRNA, *A. stirisquamum* differed from the *A. operculatum* strain K-0663 from Australia, strain CAWD42 from New Zealand, and strain TIO40 from the South China Sea in 419, 433, and 430 positions (with 68.6, 67.49, and 67.74% similarity), respectively. The *A. stirisquamum* LSU rRNA sequences differed from the *A. incoloratum* strain isolated from Australia in 414 positions (69.14% similarity). For ITS, *A. stirisquamum* differed from *A. steinii* strain TIO181 from the South China Sea and *A. gibbosum* strain Amgi0406-1CMSTAC018 from the Bahamas in 308 and 260 positions (with 45.9 and 38.1% similarity), respectively.

The ML and BI analyses based on the SSU rRNA gene sequences shown similar phylogenetic trees, and both

were generally showed low bayesian posterior probabilities / ML bootstrap support values in the early divergence of the trees. The ML tree is shown in Supplementary Fig. S1. *Amphidinium sensu stricto* including *A. carterae*, *A. cupulatisquama*, *A. fijiensis* Karafas and Tomas, *A. gibbosum*, *A. klebsii*, *A. massartii*, *A. operculatum*, *A. pseudomassartii* Karafas and Tomas, *A. steinii*, and *A. stirisquamum* were grouped together in a fully supported clade. They were sisters to a clade comprising *Gyrodinium spirale* (Bergh) Kofoid & Swezy, and *G. fusiforme* Kofoid & Swezy. *Amphidinium herdmanii* Kofoid & Swezy and *A. mootonorum* Murray & Patterson were not within the mainly *Amphidinium sensu stricto* clade, but were grouped together with *Karenia* spp., *Brachidinium capitatum* Taylor, and *Cucumeridinium* spp. in a low supported clade (Bayesian posterior probabilities / ML

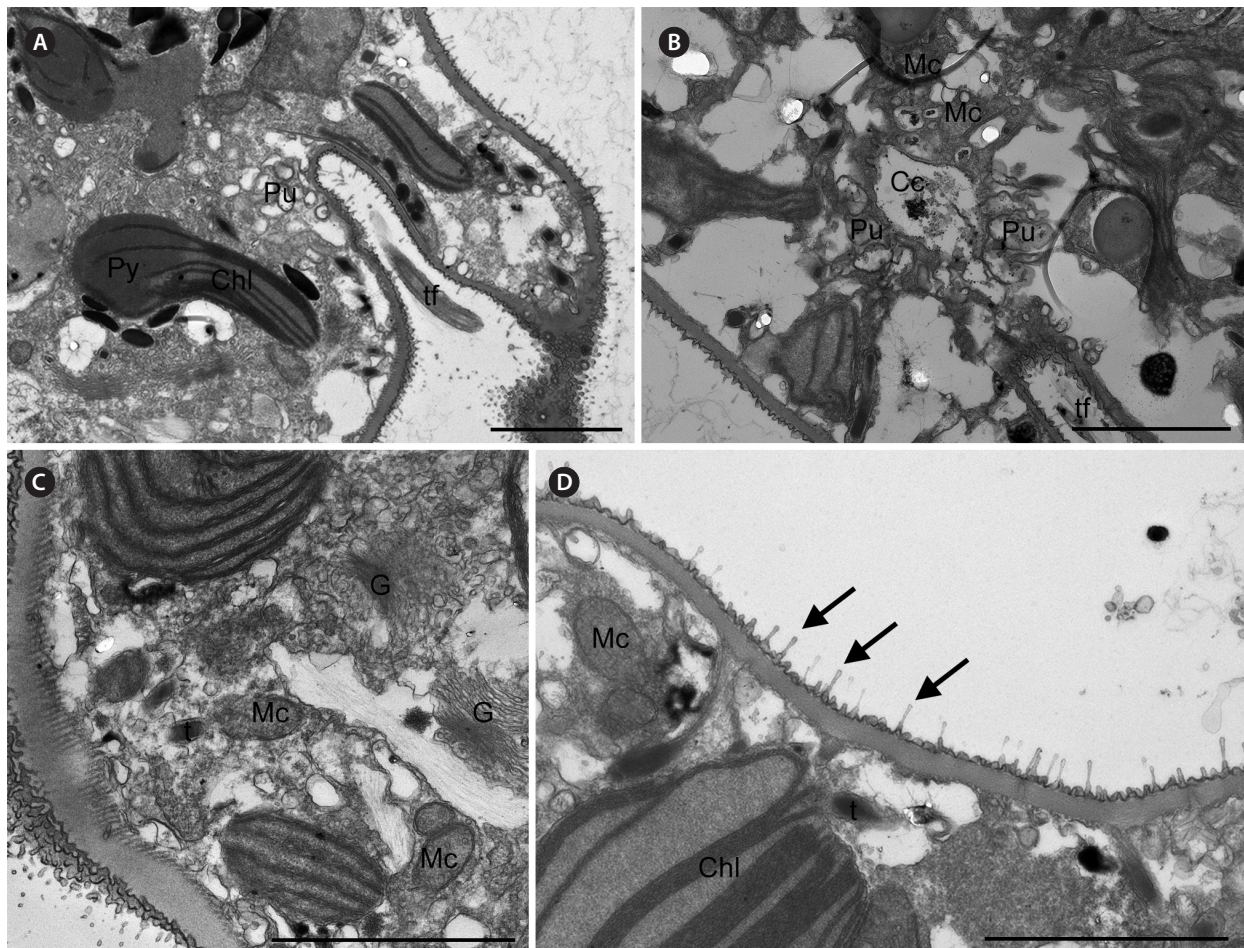


**Fig. 4.** *Amphidinium stirisquamum* sp. nov. transmission electron microscopy images. (A) Longitudinal section through a cell, showing pusule (Pu), transverse flagellum (tf) and a pyrenoid (Py) matrix is traversed by thylakoids. (B) Detail of pusule (Pu) showing the central chamber (Cc) and spherical collecting tubes, as well as mitochondria (Mc) and transverse flagellum (tf). (C) Golgi bodies (G), trichocyst (t), and mitochondria (Mc). (D) Body scales (arrows). Scale bars represent: A–D, 2  $\mu$ m.

bootstrap analysis, 0.5 / 92%).

The ML and BI analyses based on LSU rRNA gene sequences shown almost the same topology, the ML phylogeny is shown in Fig. 5. *A. stirisquamum* and *A. operculatum* were sister clades in the early divergent of *Amphidinium sensu stricto* clade. *A. incoloratum* was the second earliest branch followed by *A. steinii* Lemmermann, *A. cupulatisquama*, *A. herdmanii*, and *A. mootonorum*. The rest of the *Amphidinium sensu stricto* formed a well-resolved clade, with full support (1.0 / 100%).

The ML and BI analysis based on ITS-5.8S rRNA gene sequences generated similar phylogenetic trees, the ML tree is shown in Fig. 6. *Amphidinium sensu stricto* species were resolved in accordance with traditional morphometrics-based taxa units, which is consistent

with the LSU sequences-based phylogeny. *A. steinii* diverged early, followed by *A. stirisquamum*. The rest of the *Amphidinium* formed a well-resolved clade, with maximal support.

### Toxicity

Survival rates of *Ar. salina* exposed to *A. stirisquamum* were calculated based on the numbers of viable original individuals exposed to different culture food combinations (Table 1, Fig. 7A–F). Providing *A. stirisquamum* as a single food, either strain TIO971 or TIO955, at cell densities of 2,000, 3,000, 4,000, and 5,000 cells mL<sup>-1</sup>, negatively affected the survival rate of *Ar. salina* with extremely statistical significance ( $p < 0.01$ ) (Table 1). Providing *A. stirisquamum* as a single food at cell densities of 1,000 cells

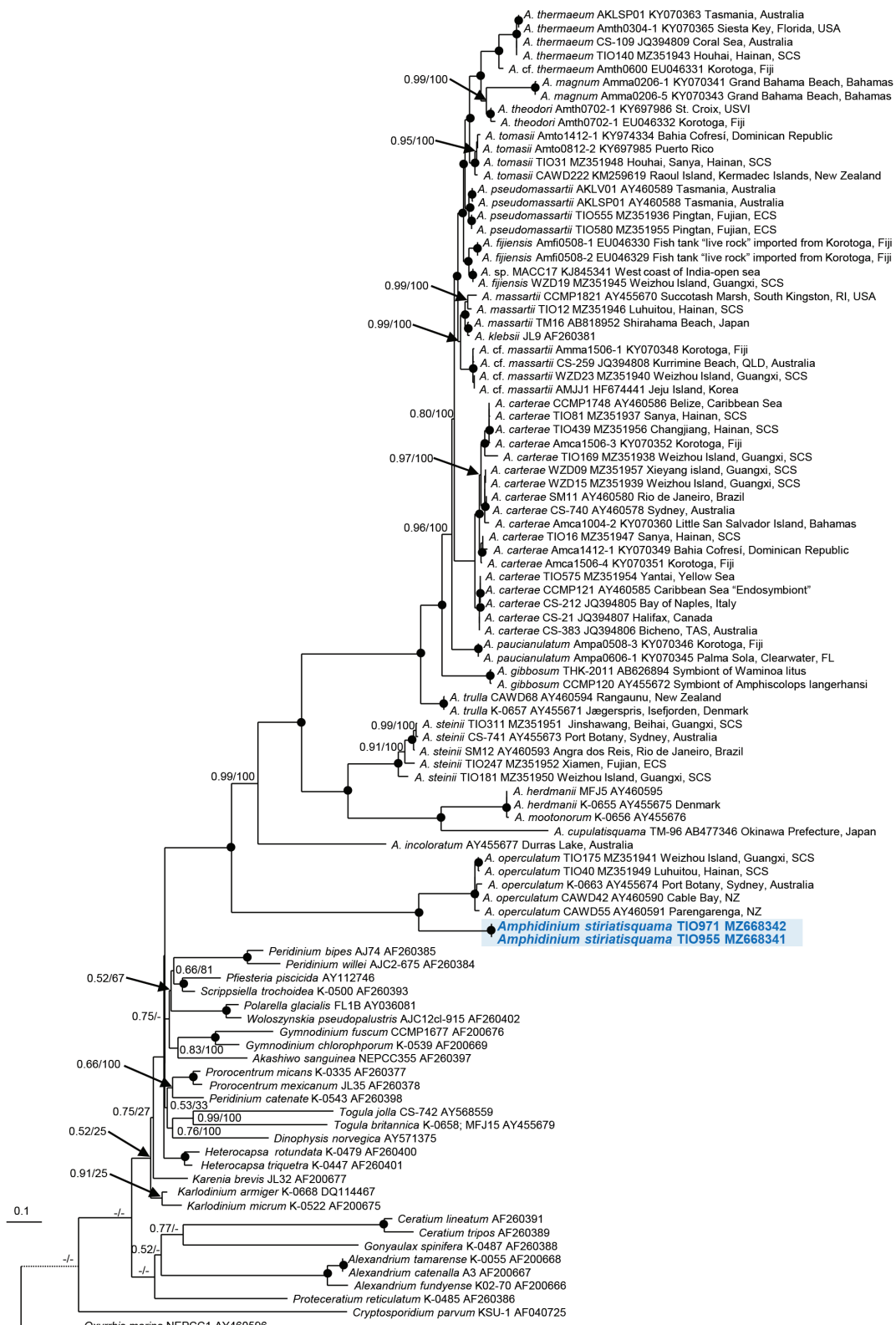


**Fig. 5.** Molecular phylogeny of *Amphidinium* inferred from partial large subunit rRNA sequences using maximum likelihood (ML). *Oxyrrhis marina* was used as outgroup. Values at nodes show the statistical support of the ML bootstrap analysis and Bayesian posterior probabilities (right, ML bootstrap support values; left, Bayesian posterior probabilities); black circles show the maximal support in ML and Bayesian inference (100% and 1.0, respectively). Posterior probabilities >0.5 and bootstrap values >50% are shown.



**Fig. 6.** Molecular phylogeny of *Amphidinium* inferred from internal transcribed spacer region sequences using maximum likelihood (ML). *Karladinium armiger* was used as the outgroup. Values at nodes shown the statistical support of the ML bootstrap analysis and Bayesian posterior probabilities (right, ML bootstrap support values; left, Bayesian posterior probabilities); black circles show the maximal support in ML and Bayesian inference (100% and 1.0, respectively). Posterior probabilities >0.5 and bootstrap values >50% are shown.

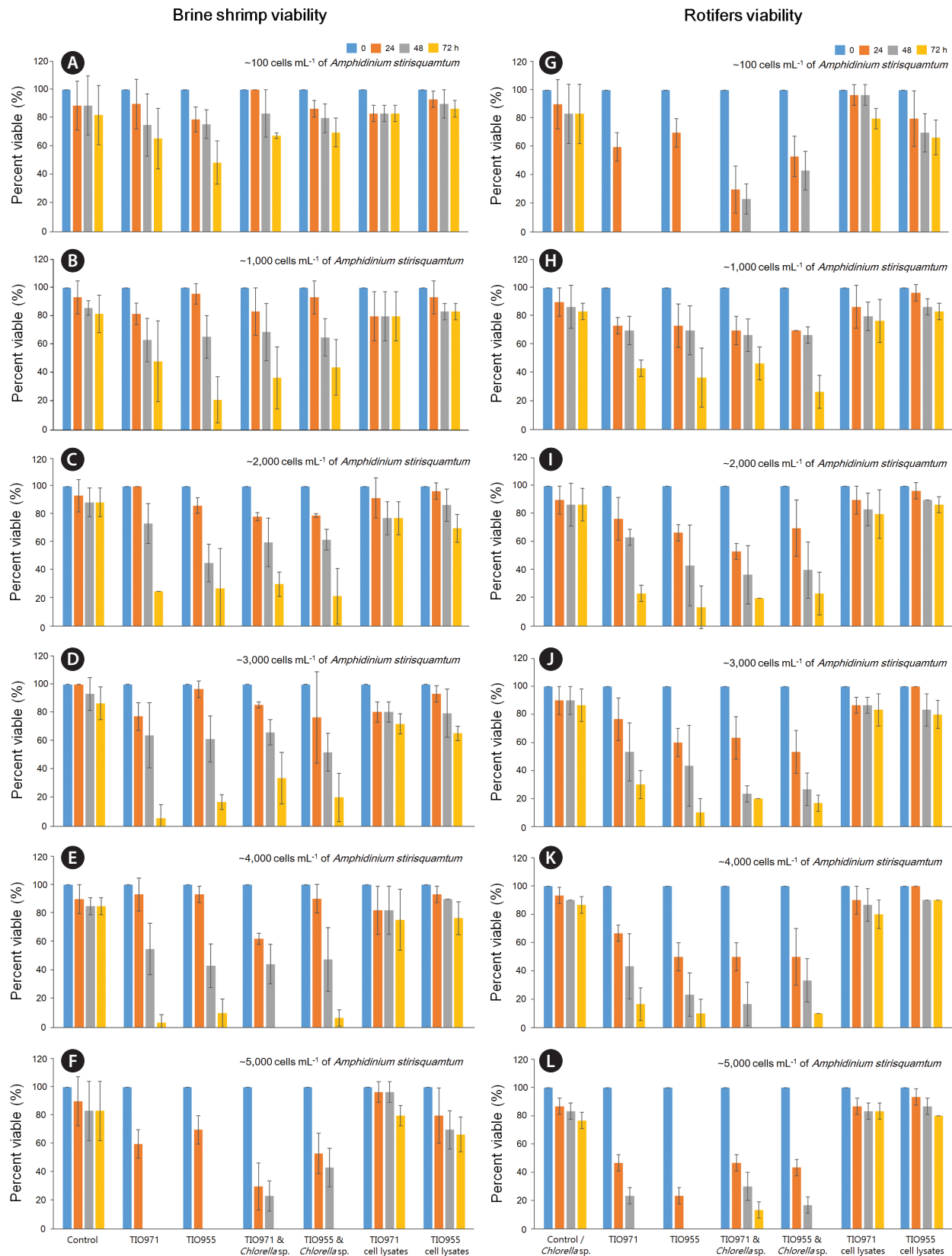


**Fig. 7.** Brine shrimp (A–F) and Rotifers (G–L) viability results at 0 (blue), 24 (orange), 48 (gray), and 72 (yellow) hours after being treated with different combinations of food sources.

$\text{mL}^{-1}$ , strain TIO955 negatively affected the survival rate of *Ar. salina* with extremely statistical significance ( $p < 0.01$ ) (Table 1), but shown no statistical significance for strain TIO971. Providing *A. stirisquamatum* as a single food, either strain TIO971 or TIO955, at cell densities of 100 cells  $\text{mL}^{-1}$  shown no statistical significance in the survival rate of *Ar. salina* compared with the control. The combined supply of *Chlorella* sp. and *A. stirisquamatum*, at cell densities of 1,000, 2,000, 3,000, 4,000, and 5,000 cells  $\text{mL}^{-1}$ , as food source also negatively affected the survival rate of *Ar. salina* with statistical significance ( $p < 0.05$ ) or extreme significance ( $p < 0.01$ ), but shown no statistical significance when cell densities at 100 cells  $\text{mL}^{-1}$  (Table 1). No significant difference was observed between liquid nitrogen freeze-thaw treated *A. stirisquamatum* culture at different cell densities and the control (Table 1).

The rotifer viable ratio was calculated and *A. stirisquamatum* was found to significantly affect the survival rate of *B. plicatilis* (Table 2, Fig. 7G–L). Providing *A. stirisquamatum* as a single food, either strain TIO971 or TIO955, at all different cell densities, negatively affected the survival rate of *Ar. salina* with statistical significance ( $p < 0.05$ ) or extreme significance ( $p < 0.01$ ) (Table 2). The combined supply of *Chlorella* sp. and *A. stirisquamatum*, at cell densities of 1,000, 2,000, 3,000, 4,000, and 5,000 cells  $\text{mL}^{-1}$ , as food source also negatively affected the survival rate of *Ar. salina* with statistical significance ( $p < 0.05$  or  $p$

$< 0.01$ ), but shown no statistical significance when cell densities at 100 cells  $\text{mL}^{-1}$  (Table 2). No significant difference was observed between all different cell densities liquid nitrogen freeze-thaw treated *A. stirisquamatum* culture and the control (Table 2).

## DISCUSSION

### Morphology

*Amphidinium stirisquamatum* is an athecate benthic dinoflagellate with minute irregular triangular-shaped epicone deflected to the left, thus fitting the description of *Amphidinium sensu stricto* (Jørgensen et al. 2004b). It is characterized by a longitudinal flagellum inserted in the lower third of the cell, icicle-shaped body scales on the cell body surface, an asymmetrical hypocone with left side longer than the right, and the presence of immotile cells (Figs 1 & 2). The longitudinal flagellum of *A. stirisquamatum* is inserted at the lower third of the cell at the beginning of the sulcus, and is not connected to the cingulum. The separation between the sulcus and cingulum distinguishes *A. stirisquamatum* from other *Amphidinium* species, except for *A. incoloratum* (*sensu* Murray and Patterson 2002) and *A. operculatum* (Table 3). *A. stirisquamatum* is an autotrophic *Amphidinium* species

**Table 1.** Two-way ANOVA analysis of the survival rates of *Artemia salina*

Experimental group	p-value / Control group					
	100 (cells $\text{mL}^{-1}$ )	1,000 (cells $\text{mL}^{-1}$ )	2,000 (cells $\text{mL}^{-1}$ )	3,000 (cells $\text{mL}^{-1}$ )	4,000 (cells $\text{mL}^{-1}$ )	5,000 (cells $\text{mL}^{-1}$ )
<i>A. stirisquamatum</i> TIO971	0.789	0.149	0.000**	0.000**	0.000**	0.000**
<i>A. stirisquamatum</i> TIO971 & <i>Chlorella</i> sp.	0.452	0.040*	0.001**	0.001**	0.000**	0.001**
<i>A. stirisquamatum</i> TIO971 cell lysates	0.956	0.829	0.664	0.651	0.893	0.703
<i>A. stirisquamatum</i> TIO955	0.329	0.000**	0.002**	0.000**	0.000**	0.000**
<i>A. stirisquamatum</i> TIO955 & <i>Chlorella</i> sp.	0.835	0.018*	0.000**	0.010**	0.000**	0.001**
<i>A. stirisquamatum</i> TIO955 cell lysates	0.977	0.991	0.175	0.226	0.893	0.821

p-value is calculated for the experimental groups in comparison to the control groups. \*Significant, \*\*Extremely significant.

**Table 2.** Two-way ANOVA analysis of the survival rates of *Brachionus plicatilis*

Experimental group	p-value / Control group					
	100 (cells $\text{mL}^{-1}$ )	1,000 (cells $\text{mL}^{-1}$ )	2,000 (cells $\text{mL}^{-1}$ )	3,000 (cells $\text{mL}^{-1}$ )	4,000 (cells $\text{mL}^{-1}$ )	5,000 (cells $\text{mL}^{-1}$ )
<i>A. stirisquamatum</i> TIO971	0.016*	0.006**	0.000**	0.003**	0.000**	0.000**
<i>A. stirisquamatum</i> TIO971 & <i>Chlorella</i> sp.	0.202	0.034*	0.000**	0.000**	0.000**	0.000**
<i>A. stirisquamatum</i> TIO971 cell lysates	0.538	0.940	0.985	0.979	0.880	0.176
<i>A. stirisquamatum</i> TIO955	0.001**	0.044*	0.003**	0.001**	0.000**	0.000**
<i>A. stirisquamatum</i> TIO955 & <i>Chlorella</i> sp.	0.490	0.000**	0.005**	0.000**	0.000**	0.000**
<i>A. stirisquamatum</i> TIO955 cell lysates	0.232	0.835	0.891	0.304	0.182	0.418

p-value is calculated for the experimental groups in comparison to the control groups. \*Significant, \*\*Extremely significant.

that is somewhat distinguishable from *A. incoloratum*, the only heterotrophic *Amphidinium sensu stricto* species devoid of chloroplasts (Murray and Patterson 2002, Jørgensen et al. 2004b). In addition, *A. stirisquamatum* differs from *A. incoloratum* regarding nucleus shape (elongated vs. round) (Murray and Patterson 2002). *Amphidinium stirisquamatum* differs from *A. operculatum* in respect to the cell shape (oval shaped with the broadest width at the cell center vs. pear shaped with the broadest width at the posterior), body scales (icicle-shaped body scales vs. no body scale), “stigma” or “dark spot” (invisible under light microscopy [LM] vs. often visible under LM), and a hypocone shape (left side longer than the right vs. equal length of both sides, both sides show obviously convex shape vs. convex only on the right side while the left side is almost straight) (Claparède and Lachmann 1859, Murray et al. 2004).

Under SEM, icicle-shaped body scales were observed on the surface of the *A. stirisquamatum* cell body (Fig. 2A–E) when osmium tetroxide was used for fixation, but these were stripped away when glutaraldehyde was used for fixation (Fig. 2F & G). SEM is a valuable tool for determining the presence of scales, but cannot be used for determining absence if they are not observed, due to the loss of scale by different fixation methods (Sekida et al. 2003, Karafas et al. 2017, this study). Body scale possess or not as well as their three-dimensional structure are one of the important morphological features used to identify *Amphidinium* species (Tamura et al. 2009, Murray et al. 2012, Karafas et al. 2017). To date, two types of body scales have been reported in four *Amphidinium* species: in *A. cupulatisquama* the body scales are cup-shaped with distinct three-dimensionality (Tamura et al. 2009), in *A. massartii* (*A. massartii* and *A. cf. massartii*), *A. paucianulatum*, and *A. theodori* the scales are doughnut-shaped or ring-like (Sekida et al. 2003, Murray et al. 2012, Lee et al. 2013, Karafas et al. 2017). The present study reports a novel type of body scale in *A. stirisquamatum*, which is icicle-shaped and distributed throughout the cell body (Figs 2 & 3). The cup-shaped scales in *A. cupulatisquama* and the icicle-shaped scales in *A. stirisquamatum* seem to be unique to date (Tamura et al. 2009, this study), although doughnut-shaped scales have been found in *A. massartii* (including *A. cf. massartii*), *A. paucianulatum*, and *A. theodori* (Murray et al. 2012, Lee et al. 2013, Karafas et al. 2017). Nevertheless, an unambiguous feature that can be used to differentiate *Amphidinium* species is rare and risky, and some characteristics can even overlap among species (Murray and Patterson 2002, Jørgensen et al. 2004b, Murray et al. 2004). Therefore, a combination

of characteristics seems to be the best approach to differentiate among *Amphidinium* species (Karafas et al. 2017). The molecular tree based on SSU and LSU rRNA indicated that *A. stirisquamatum* was grouped together with the type species of *Amphidinium*, *A. operculatum*, in a fully supported clade (Fig. 5, Supplementary Fig. S1). They are distantly related to other species of body scale-bearing *Amphidinium*, implying independent evolution of body scales.

Under TEM, *A. stirisquamatum* have a typical dinophyceae ultrastructure, that is, a large dinokaryon with condensed chromosomes, single chloroplast, numerous mitochondria with tubular cristae, trichocysts, and Golgi bodies (Table 3, Figs 3 & 4). The pusule system of *A. stirisquamatum* is a complex of vesicles comprising a central chamber and spherical collecting tubes, lying near the origin of the transverse and longitudinal flagella, respectively (Fig. 4A & B). The similar pusule structure also reported in *A. operculatum* (Murray et al. 2004), *A. incoloratum* (Murray and Patterson 2002), *A. carterae* (as *A. rhynchocephalum* Anissimowa) (Farmer and Roberts 1989), and *A. cupulatisquama* (Tamura et al. 2009) implies that it may be a common cytoarchitecture of *Amphidinium*. The pusule connects to a chamber adjacent to the flagellar canal (Maranda and Shimizu 1996), or directly fuses with the membrane of the flagellar pocket (Murray et al. 2004, Lee et al. 2013), implying that it might be related to flagellar motility. Under TEM, an unknown organelle was identified behind the sulcus and the nucleus (Fig. 3B) that was not observed under LM. It was somewhat different from the “stigma” or “dark spot” in *A. operculatum*, which is often visible under LM, and located in the cell center just above the beginning of the sulcus (Claparède and Lachmann 1859, Grell and Wohlfarth-Bottermann 1957). The organelle function of “stigma”, “dark spot”, or the “unknown organelle” reported here remains unidentified, and their taxonomic significance requires validation.

## Phylogeny

Phylogeny analyses based on either SSU rRNA or LSU rRNA gene sequences shown that the new *A. stirisquamatum* is grouped with the type species *A. operculatum*, as well as the other *Amphidinium sensu stricto* species forming a well-supported clade (Fig. 5, Supplementary Fig. S1). This result supports the placement of *A. stirisquamatum* in the genus *Amphidinium sensu stricto*. Phylogenetic analysis of partial LSU rRNA (domains D1–D6) revealed that *Amphidinium sensu stricto* was monophy-

**Table 3.** Morphological features of selected *Amphidinium* sensu stricto species compiled from the results of the present study and the published literature

	<i>A. stirisquamum</i>	<i>A. operculatum</i>	<i>A. incoloratum</i>	<i>A. gibbosum</i>	<i>A. carterae</i>	<i>A. massartii</i>	<i>A. cupulatisquama</i>
Length (L, $\mu\text{m}$ )	30.3–37.0	29–50	27–38	31–43	10–20	6–29	30–59
Width (W, $\mu\text{m}$ )	24.1–30.2	21–28	17–24	19–23	9–13	5–21	19–43
L/W	1.20–1.37	-	1.3–1.6	1.6–1.9	-	-	-
Shape	Oval shaped	Pear shaped	Broadly oval to egg-shaped	Elongate to heart shaped	Round to elliptical shaped	Round, oval, elliptical shaped	Oval shaped
Eposome	Triangle, left-deflecting	Irregular triangular, left-deflecting	Triangle, left-deflecting	Tongue-like, pointing left	Crescent, flat, left-deflecting	Crescent, flat, left-deflecting	Boomerang-shaped
Hyposome	Asymmetrical, longer left side, both sides are convex, the broadest width in the cell center	Right side is convex, left is almost straight, the broadest width between the cell center and the posterior end	Longer left side, the left side is relatively straight and the right side is convex	Two asymmetrical lobes, dorsoventrally compressed, "humpbacked"	Symmetrical	Asymmetrical, the anterior shoulders are slightly higher at the left side	Oval, right side is rather straight in comparison with the left side
Antapex	Broadly, and pointed at the left side	Broadly rounded	Round, elliptical	Pointed	Round, elliptical	Slightly pointed	Slightly pointed
LF insertion	Lower 1/3	Lower 1/3	Lower 1/3	Anterior 1/3	Mid 1/3	Mid 1/3	Anterior 1/3
Body scales	Icicle-shaped	None	-	None	None	Doughnut-shaped or ring-like	Cup-shaped with distinct three-dimensionality
Asexual division	Motile	Motile	-	Motile	Motile	Motile	Motile
Nucleus	Elongated, posteriorly located	Crescent shaped or oval, posteriorly located	Round, posteriorly located	Ovoid-crescent, posteriorly located	Round, posteriorly located	Rounded or crescent-shaped, posteriorly located	Spherical, posteriorly located
Plastid	Single, yellow-golden, radiated from centrally located pyrenoids and branched peripherally	Multiple, yellow-brown and elongated, radiate to the cell periphery	None	Single or multiple, stellate, golden-brown	Single with multiple lobes radiation out from the center of the cell, yellow-brown	Single yellow-green plastid with several narrow lobes, radiating out from the cell center	Single chloroplast, yellow-brown with many thread-like lobes radiating from the central pyrenoid
Pyrenoid	Numerous, single-stalked, centrally located	None	-	Single, multi-stalked, centrally located	Central ring-like starch-sheathed pyrenoid	One or two central ring-like starch-sheathed pyrenoid	One pyrenoid, situated just anterior to the center

**Table 3.** continued.

	<i>A. stirisquantum</i>	<i>A. operculatum</i>	<i>A. incoloratum</i>	<i>A. gibbosum</i>	<i>A. carterae</i>	<i>A. massartii</i>	<i>A. cupulatisquama</i>
Pusule	Two, lying in close proximity to the origin of the transverse and longitudinal flagella	Two, lying in close proximity to the origin of the transverse and longitudinal flagella	Two pusules present: one large, obvious, to the right of the anterior end of the sulcus, the other small, below the origin of the cingulum	Filled subspherical vesicles connected to a single membrane-branched collecting chamber opening on the flagellar canal via a narrow opening surrounded by a fibrous collar	Two, adjacent to each of the two flagellar pockets	Present, nearby flagellar	One, consists of a central chamber and spherical collecting tubes, which radiate from it
Mitochondria	Numerous, elongated, scattered	Present	-	Numerous, elongated, scattered	Scattered throughout the cytoplasm	Present	Present
Golgi bodies	Numerous, multiple cisternae, scattered	-	-	4+ cisternae, outside the polysaccharide cap	Numerous, anteriorly located	Present	Present
Accumulation body	Many lipid globules	Colorless globules	Many colorless lipid globules	Polysaccharide cap and inclusions, lipid globules	-	Starch grains	Numerous lipid and starch grains
Trichocysts	Numerous, at the cell periphery	-	-	Numerous, at the cell periphery and between nucleus and pyrenoid	-	Present	Present
Reference	Grell and Wohlfarth-Bottermann (1957), Murray et al. (2004)	Murray and Patterson (2002)	Murray et al. (2004), Maranda and Shimizu (1996)	Murray et al. (2004), Lee et al. (2013)	Murray et al. (2004), Lee et al. (2013)	Murray et al. (2004, 2012), Lee et al. (2013)	Murray et al. (2004, 2012), Lee et al. (2013)

letic with high support (Jørgensen et al. 2004b, Murray et al. 2005, this study). In LSU rRNA sequence-based phylogenetic tree, *A. stirisquamatum* is most closely linked to *A. operculatum*, and this is also reflected in the morphology, for example they share the same characteristic of longitudinal flagellum insertion in the lower third of the cell. *Amphidinium incoloratum* is in the basal position in the LSU rRNA sequence-based phylogeny (Jørgensen et al. 2004b, Karafas et al. 2017). The evolutionary relationship is rather ambiguous, and the *A. operculatum* / *A. stirisquamatum* clade shifted to the basal position when the new *A. stirisquamatum* sequences were introduced (Fig. 5). More *A. incoloratum*, *A. operculatum*, and *A. striatisquama* sequences are needed to clarify their evolutionary relationship. ITS sequence-based phylogeny has been proven valuable for distinguish specific and sub-specific relationships of dinoflagellate (Hillis and Dixon 1991, Yoshida et al. 2003, Hunter et al. 2007, Stern et al. 2012). *Amphidinium* species were resolved in accordance with traditional morphometric-based taxa units, which is consistent with the LSU rRNA sequence-based phylogeny (Figs 5 & 6). More ITS sequences are needed, especially for the type species, *A. operculatum*, to clarify the evolutionary relationship of *Amphidinium sensu stricto*.

## Toxicity

Brine shrimp and rotifers are important primary grazers in shallow coastal environments (Hernroth 1983). They are an optimal live food item for early larval culture stages of shrimp, crab, and fish (Sorgeloos et al. 2001, Sakakura 2017, Quy et al. 2018, Sterzelecki et al. 2021). In addition, both *Ar. salina* and *B. plicatilis* have a widespread distribution, short life cycle, non-selective grazing, and sensitivity to toxins, and thus are widely used for marine harmful dinoflagellates toxicity tests (Baig et al. 2006, Yan et al. 2009, Faimali et al. 2012, Lin et al. 2016, Neves et al. 2017). *Amphidinium* is one of the most abundant members of benthic dinoflagellates in marine intertidal ecosystems (Dodge and Hart-Jones 1982, Murray and Patterson 2002). In normal naturally water, the abundance of *Amphidinium* in sandy areas reaches up to 507 cells per 100 cm<sup>2</sup> (Yong et al. 2018), and on the macroalgal up to 410 cells g<sup>-1</sup> wet weight macroalgal (Kim et al. 2011). In *Amphidinium* bloom water, the abundance of *Amphidinium* even reaches  $1.80 \times 10^5$  cells mL<sup>-1</sup> (Murray et al. 2015). Here, we report that providing *A. stirisquamatum* as a single food source at the cell density of 100 cells mL<sup>-1</sup> or more negatively affected the survival rate of *Ar. salina* and *B. plicatilis* with

statistical significance (Tables 1 & 2). The percentage of survival of *Ar. salina* and *B. plicatilis* reversely proportional to cell density of *A. stirisquamatum* (Fig. 7). The benthic dinoflagellate *Prorocentrum lima* (Ehrenberg) F. Stein, *Gambierdiscus excentricus* S. Fraga & *Ostreopsis cf. ovata* Y. Fukuyo also significantly affected the *Ar. salina* survival rate with a 100% mortality after 7 h of exposure (Neves et al. 2017). The present results suggested that the toxic *Amphidinium* were able to induce similar effects on the survival of brine shrimp and rotifers. *Prorocentrum* Ehrenberg, *Gambierdiscus* Adachi & Fukuyo, *Ostreopsis* Schmidt, *Coolia* Meunier, and *Amphidinium* are the most abundant members of toxic benthic dinoflagellates and a primary organic source in marine intertidal and neritic sandy ecosystems (Murray and Patterson 2002, Zhang 2015, Gómez et al. 2016, Gémin et al. 2019, Nishimura et al. 2019). Their toxic effect causes sub-lethal effects and/or even mortality of their primary grazers, and make them easier targets for the next consumers. Meanwhile, the toxicity resulting from the bio-accumulation of benthic toxic dinoflagellates through marine food webs consequently affects consumers at higher trophic levels, including fish, seabirds, and marine mammals (Turner and Tester 1997).

Different concentrations (10, 100, and 1,000 cells mL<sup>-1</sup>) of the *A. carterae* lysed cell suspension did not appear to show any significant toxicity to *Ar. salina* (Baig et al. 2006). The cell-free medium from cultures of *P. lima*, *O. cf. ovata*, and *G. excentricus* (~200 cells mL<sup>-1</sup>) did not significantly affect *Ar. salina* survival rate during acute exposure (Neves et al. 2017), but cell-free medium from cultures with higher abundances of *O. cf. ovata* (~4,000 cells mL<sup>-1</sup>) was harmful to the nauplii of *Ar. salina* (Faimali et al. 2012). In the present study, the liquid nitrogen freeze-thaw treated *A. stirisquamatum* (TIO955 and TIO971) culture media at the cell density of 100 to 5,000 cell mL<sup>-1</sup> did not show any significant toxicity to the *Ar. salina* or *B. plicatilis* (Tables 1 & 2, Fig. 7). This implies that either ruptured cells or cultured media exhibited no toxicity to *Ar. salina* and *B. plicatilis*. We propose that the toxins are originally produced intracellularly, and that when cell lysis occurred and toxins leaked out to the medium, their concentration was insufficient to affect the survival of *Ar. salina* and *B. plicatilis*.

It has been reported that lipophilic secondary metabolites derived from microalgae can be sources of biologically active substances, including toxins (Parrish et al. 1998, Rossini 2014, Dang et al. 2015). The toluene extract of cultured *A. carterae* was found to be toxic to pearl oysters, and the bioassay-guided purification of the

toluene soluble fraction resulted in the isolation of a new glycoglycerolipid (Wu et al. 2005). A gill-damaging and therefore fish-poisoning or ichthyotoxic effect has been correlated with a bloom of *A. carterae* in a coastal lagoon in Sydney, Australia (Murray et al. 2015). Our result increases knowledge of the direct toxic effects of *Amphidinium* on zooplankton, i.e., *Ar. salina* and *B. plicatilis*, which are widely used as model organisms in toxicological evaluation (Nunes et al. 2006, Neves et al. 2017, Li et al. 2020, this study). Microalgae exhibit a diversity of chemical defenses that can affect the feeding and fitness of zooplankton consumers (Prince et al. 2006). Further studies are necessary to identify why only live cells can affect the survival of brine shrimp and rotifers, as well as the type of toxic compounds produced by *Amphidinium*, and how they affect the survival rate of their primary grazers.

## ACKNOWLEDGEMENTS

This work was supported by the National Natural Science Foundation of China (41806154), the Scientific Research Foundation of Third Institute of Oceanography, MNR (2017023), the National Key Research and Development Program of China (2019YFE0124700) and the Youth Innovation Project of Xiamen 3502Z20206095. The authors would like to thank two anonymous reviewers whose comments and suggestions greatly improved the early version of the manuscript.

## CONFLICTS OF INTEREST

The authors declare that they have no potential conflicts of interest.

## SUPPLEMENTARY MATERIALS

**Supplementary Fig. S1.** Molecular phylogeny inferred from partial small subunit rRNA sequences using maximum likelihood (ML) (<https://e-algae.org>).

**Supplementary Video S1.** *Amphidinium stirisquamum* sp. nov. strain TIO971 living cells (<https://e-algae.org>).

## REFERENCES

Adachi, M., Sake, Y. & Ishida, Y. 1996. Analysis of *Alexandri-*

*um* (Dinophyceae) species using sequences of the 5.8S ribosomal DNA and internal transcribed spacer regions. *J. Phycol.* 32:424–432.

Baig, H. S., Saifullah, S. M. & Dar, A. 2006. Occurrence and toxicity of *Amphidinium carterae* Hulbert in the North Arabian Sea. *Harmful Algae* 5:133–140.

Berdalet, E., Tester, P. A., Chinain, M., Fraga, S., Lemée, R., Litaker, W., Penna, A., Usup, G., Vila, M. & Zingone, A. 2017. Harmful algal blooms in benthic systems. *Oceanography* 30:36–45.

Boc, A., Diallo, A. B. & Makarenkov, V. 2012. T-REX: a web server for inferring, validating and visualizing phylogenetic trees and networks. *Nucleic Acids Res.* 40:W573–W579.

Calado, A. J. & Moestrup, Ø. 2005. On the freshwater dinoflagellates presently included in the genus *Amphidinium*, with a description of *Prosoaulax* gen. nov. *Phycologia* 44:112–119.

Carroll, H., Beckstead, W., O'Connor, T., Ebbert, M., Clement, M., Snell, Q. & McClellan, D. 2007. DNA reference alignment benchmarks based on tertiary structure of encoded proteins. *Bioinformatics* 23:2648–2649.

Claparède, E. & Lachmann, J. 1859. Études sur les infusoires et les rhizopodes. *Mém. Inst. Natl. Genevois* 6:261–482.

Dang, L. -X., Li, Y., Liu, F., Zhang, Y., Yang, W. -D., Li, H. -Y. & Liu, J. -S. 2015. Chemical response of the toxic Dinoflagellate *Karenia mikimotoi* against grazing by three species of zooplankton. *J. Eukaryot. Microbiol.* 62:470–480.

Darriba, D., Taboada, G. L., Doallo, R. & Posada, D. 2012. jModelTest 2: more models, new heuristics and parallel computing. *Nat. Methods* 9:772.

Daugbjerg, N., Hansen, G., Larsen, J. & Moestrup, Ø. 2000. Phylogeny of some of the major genera of dinoflagellates based on ultrastructure and partial LSU rDNA sequence data, including the erection of three new genera of unarmoured dinoflagellates. *Phycologia* 39:302–317.

De Jonge, V. N. & Van Beuselom, J. E. E. 1992. Contribution of resuspended microphytobenthos to total phytoplankton in the EMS estuary and its possible role for grazers. *Neth. J. Sea Res.* 30:91–105.

Dodge, J. D. & Hart-Jones, B. 1982. *Marine dinoflagellates of the British Isles*. Her Majesty's Stationery Office, London, 303 pp.

Dolapsakis, N. P. & Economou-Amilli, A. 2009. A new marine species of *Amphidinium* (Dinophyceae) from Thermaikos Gulf, Greece. *Acta Protozool.* 48:153–170.

Echigoya, R., Rhodes, L., Oshima, Y. & Satake, M. 2005. The structures of five new antifungal and hemolytic amphidinol analogs from *Amphidinium carterae* collected in New Zealand. *Harmful Algae* 4:383–389.

- Facca, C., Sfriso, A. & Socal, G. 2002. Changes in abundance and composition of phytoplankton and microphytobenthos due to increased sediment fluxes in the Venice lagoon, Italy. *Estuar. Coast. Shelf Sci.* 54:773–792.
- Faimali, M., Giussani, V., Piazza, V., Garaventa, F., Corrà, C., Asnaghi, V., Privitera, D., Gallus, L., Cattaneo-Vietti, R., Mangialajo, L. & Chiantore, M. 2012. Toxic effects of harmful benthic dinoflagellate *Ostreopsis ovata* on invertebrate and vertebrate marine organisms. *Mar. Environ. Res.* 76:97–107.
- Farmer, M. A. & Roberts, K. R. 1989. Comparative analyses of the dinoflagellate flagellar apparatus. III. Freeze substitution of *Amphidinium rhynchocephalum*. *J. Phycol.* 25:280–292.
- Forster, D., Dunthorn, M., Mahé, F., Dolan, J. R., Audic, S., Bass, D., Bittner, L., Boutte, C., Christen, R., Claverie, J. -M., Decelle, J., Edvardsen, B., Egge, E., Eikrem, W., Gobet, A., Kooistra, W. H. C. F., Logares, R., Massana, R., Montresor, M., Not, F., Ogata, H., Pawłowski, J., Perne, M. C., Romac, S., Shalchian-Tabrizi, K., Simon, N., Richards, T. A., Santini, S., Sarno, D., Siano, R., Vaulot, D., Wincker, P., Zingone, A., De Vargas, C. & Stoeck, T. 2016. Benthic protists: the undercharted majority. *FEMS Microbiol. Ecol.* 92:fiw120.
- Gárate-Lizárraga, I., González-Armas, R., Verdugo-Díaz, G., Okolodkov, Y. B., Pérez-Cruz, B. & Díaz-Ortíz, J. A. 2019. Seasonality of the dinoflagellate *Amphidinium* cf. *carterae* (Dinophyceae: Amphidiniales) in Bahía de la Paz, Gulf of California. *Mar. Pollut. Bull.* 146:532–541.
- Gémén, M. -P., Réveillon, D., Hervé, F., Pavaux, A. -S., Tharraud, M., Séchet, V., Bertrand, S., Lemée, R. & Amzil, Z. 2019. Toxin content of *Ostreopsis* cf. *ovata* depends on bloom phases, depth and macroalgal substrate in the NW Mediterranean Sea. *Harmful Algae* 92:101727.
- Gómez, F., Qiu, D., Otero-Morales, E., Lopes, R. M. & Lin, S. 2016. Circumtropical distribution of the epiphytic dinoflagellate *Coolia malayensis* (Dinophyceae): morphology and molecular phylogeny from Puerto Rico and Brazil. *Phycol. Res.* 64:194–199.
- Grell, K. G. & Wohlfarth-Bottermann, K. E. 1957. Licht- und elektronenmikroskopische untersuchungen an dem Dinoflagellaten *Amphidinium elegans* n. sp. *Z. Zellforsch. Mikrosk. Anat.* 47:7–17.
- Guillard, R. R. L. & Ryther, J. H. 1962. Studies of marine planktonic diatoms. I. *Cyclotella nana* Hustedt, and *Detonula confervacea* (Cleve) Gran. *Can. J. Microbiol.* 8:229–239.
- Guiry, M. D. & Guiry, G. M. 2021. AlgaeBase. World-wide electronic publication, National University of Ireland, Galway. Available from: <http://www.algaebase.org>. Accessed Oct 1, 2021.
- Hall, T. A. 1999. BioEdit: a user-friendly biological sequence alignment editor and analysis program for Windows 95/98/NT. *Nucleic Acids Symp. Ser.* 41:95–98.
- Hernroth, L. 1983. Marine pelagic rotifers and tintinnids: important trophic links in the spring plankton community of the Gullmar Fjord, Sweden. *J. Plankton Res.* 5:835–846.
- Hillis, D. M. & Dixon, M. T. 1991. Ribosomal DNA: molecular evolution and phylogenetic inference. *Q. Rev. Biol.* 66:411–453.
- Hoppenrath, M., Murray, S., Sparmann, S. F. & Leander, B. S. 2012. Morphology and molecular phylogeny of *Ankitrodinium* gen. nov. (Dinophyceae), a new genus of marine sand-dwelling dinoflagellates formerly classified within *Amphidinium*. *J. Phycol.* 48:1143–1152.
- Hoppenrath, M., Murray, S. A., Chomérat, N. & Horiguchi, T. 2014. *Marine benthic Dinoflagellates: unveiling their worldwide biodiversity*. Schweizerbart, Stuttgart, 276 pp.
- Horiguchi, T., Tamura, M., Katsumata, K. & Yamaguchi, A. 2012. *Testudodinium* gen. nov. (Dinophyceae), a new genus of sand-dwelling dinoflagellates formerly classified in the genus *Amphidinium*. *Phycol. Res.* 60:137–149.
- Huang, S.- J., Kuo, C. -M., Lin, Y. -C., Chen, Y. -M. & Lu, C. -K. 2009. Carterao E, a potent polyhydroxyl ichthyotoxin from the dinoflagellate *Amphidinium carterae*. *Tetrahedron Lett.* 50:2512–2515.
- Huang, X. -C., Zhao, D., Guo, Y. -W., Wu, H. -M., Lin, L. -P., Wang, Z. -H., Ding, J. & Lin, Y. -S. 2004a. Lingshuiol, a novel polyhydroxyl compound with strongly cytotoxic activity from the marine dinoflagellate *Amphidinium* sp. *Bioorg. Med. Chem. Lett.* 14:3117–3120.
- Huang, X. -C., Zhao, D., Guo, Y. -W., Wu, H. -M., Trivellone, E. & Cimino, G. 2004b. Lingshuiols A and B, two new polyhydroxy compounds from the Chinese marine dinoflagellate *Amphidinium* sp. *Tetrahedron Lett.* 45:5501–5504.
- Hunter, R. L., Lajeunesse, T. C. & Santos, S. R. 2007. Structure and evolution of the rDNA internal transcribed spacer (ITS) region 2 in the symbiotic dinoflagellates (*Symbiodinium*, Dinophyta). *J. Phycol.* 43:120–128.
- Inuzuka, T., Yamada, K. & Uemura, D. 2014. Amdigenols E and G, long carbon-chain polyol compounds, isolated from the marine dinoflagellate *Amphidinium* sp. *Tetrahedron Lett.* 55:6319–6323.
- Jørgensen, M. F., Murray, S. & Daugbjerg, N. 2004a. A new genus of athecate interstitial dinoflagellates, *Togula* gen. nov., previously encompassed within *Amphidinium sensu lato*: inferred from light and electron microscopy and phylogenetic analyses of partial large subunit ribosomal DNA sequences. *Phycol. Res.* 52:284–299.

- Jørgensen, M. E., Murray, S. & Daugbjerg, N. 2004b. *Amphidinium* revisited. I. Redefinition of *Amphidinium* (Dinophyceae) based on cladistic and molecular phylogenetic analyses. *J. Phycol.* 40:351–365.
- Karafas, S., Teng, S. T., Leaw, C. P. & Alves-De-Souza, C. 2017. An evaluation of the genus *Amphidinium* (Dinophyceae) combining evidence from morphology, phylogenetics, and toxin production, with the introduction of six novel species. *Harmful Algae* 68:128–151.
- Katoh, K. & Standley, D. M. 2013. MAFFT multiple sequence alignment software version 7: improvements in performance and usability. *Mol. Biol. Evol.* 30:772–780.
- Kim, H. S., Yih, W., Kim, J. H., Myung, G. & Jeong, H. J. 2011. Abundance of epiphytic dinoflagellates from coastal waters off Jeju Island, Korea During Autumn 2009. *Ocean Sci. J.* 46:205.
- Kobayashi, J., Shigemori, H., Ishibashi, M., Yamasu, T., Hirata, H. & Sasaki, T. 1991. Amphidinolides G and H: new potent cytotoxic macrolides from the cultured symbiotic dinoflagellate *Amphidinium* sp. *J. Org. Chem.* 56:5221–5224.
- Lee, K. H., Jeong, H. J., Park, K., Kang, N. S., Yoo, Y. D., Lee, M. J., Lee, J. -W., Lee, S., Kim, T., Kim, H. S. & Noh, J. H. 2013. Morphology and molecular characterization of the epiphytic dinoflagellate *Amphidinium massartii*, isolated from the temperate waters off Jeju Island, Korea. *Algae* 28:213–231.
- Li, X. -D., Wang, X. -Y., Xu, M. -E., Jiang, Y., Yan, T. & Wang, X. -C. 2020. Progress on the usage of the rotifer *Brachionus plicatilis* in marine ecotoxicology: a review. *Aquat. Toxicol.* 229:105678.
- Lin, J., Yan, T., Zhang, Q. & Zhou, M. 2016. Impact of several harmful algal bloom (HAB) causing species, on life history characteristics of rotifer *Brachionus plicatilis* Müller. *Chin. J. Oceanol. Limnol.* 34:642–653.
- Lucas, C. H., Widdows, J., Brinsley, M. D., Salkeld, P. N. & Herman, P. M. J. 2000. Benthic-pelagic exchange of microalgae at a tidal flat. 1. Pigment analysis. *Mar. Ecol. Prog. Ser.* 196:59–73.
- Maranda, L. & Shimizu, Y. 1996. *Amphidinium operculatum* var. nov. *gibbosum* (Dinophyceae), a free-swimming marine species producing cytotoxic metabolites. *J. Phycol.* 32:873–879.
- Martínez, K. A., Lauritano, C., Druka, D., Romano, G., Grohmann, T., Jaspars, M., Martín, J., Díaz, C., Cautain, B., de La Cruz, M., Ianora, A. & Reyes, F. 2019. Amphidinol 22, a new cytotoxic and antifungal amphidinol from the Dinoflagellate *Amphidinium carterae*. *Mar. Drugs* 17:385.
- Medlin, L., Elwood, H. J., Stickel, S. & Sogin, M. L. 1988. The characterization of enzymatically amplified eukaryotic 16S-like rRNA-coding regions. *Gene* 71:491–499.
- Murray, S., Flø Jørgensen, M., Daugbjerg, N. & Rhodes, L. 2004. *Amphidinium* revisited. II. Resolving species boundaries in the *Amphidinium operculatum* species complex (Dinophyceae), including the descriptions of *Amphidinium trulla* sp. nov. and *Amphidinium gibbosum* comb. nov. *J. Phycol.* 40:366–382.
- Murray, S., Flø Jørgensen, M., Ho, S. Y. W., Patterson, D. J. & Jermiin, L. S. 2005. Improving the analysis of Dinoflagellate phylogeny based on rDNA. *Protist* 156:269–286.
- Murray, S. & Patterson, D. 2002. The benthic dinoflagellate genus *Amphidinium* in south-eastern Australian waters, including three new species. *Eur. J. Phycol.* 37:279–298.
- Murray, S. A., Garby, T., Hoppenrath, M. & Neilan, B. A. 2012. Genetic diversity, morphological uniformity and polyketide production in dinoflagellates (*Amphidinium*, Dinoflagellata). *PLoS ONE* 7:e38253.
- Murray, S. A., Kohli, G. S., Farrell, H., Spiers, Z. B., Place, A. R., Dorantes-Aranda, J. J. & Ruszczyk, J. 2015. A fish kill associated with a bloom of *Amphidinium carterae* in a coastal lagoon in Sydney, Australia. *Harmful Algae* 49:19–28.
- Neves, R. A. F., Fernandes, T., dos Santos, L. N. & Nascimento, S. M. 2017. Toxicity of benthic dinoflagellates on grazing, behavior and survival of the brine shrimp *Artemia salina*. *PLoS ONE* 12:e0175168.
- Nishimura, T., Uchida, H., Noguchi, R., Oikawa, H., Suzuki, T., Funaki, H., Ihara, C., Hagino, K., Arimitsu, S., Tanii, Y., Abe, S., Hashimoto, K., Mimura, K., Tanaka, K., Yanagida, I. & Adachi, M. 2019. Abundance of the benthic dinoflagellate *Prorocentrum* and the diversity, distribution, and diarrhetic shellfish toxin production of *Prorocentrum lima* complex and *P. caipirignum* in Japan. *Harmful Algae* 96:101687.
- Nunes, B. S., Carvalho, F. D., Guilhermino, L. M. & Van Stappen, G. 2006. Use of the genus *Artemia* in ecotoxicity testing. *Environ. Pollut.* 144:453–462.
- Nuzzo, G., Cutignano, A., Sardo, A. & Fontana, A. 2014. Antifungal amphidinol 18 and its 7-sulfate derivative from the marine dinoflagellate *Amphidinium carterae*. *J. Nat. Prod.* 77:1524–1527.
- Parrish, C. C., Bodennec, G. & Gentien, P. 1998. Haemolytic glycoglycerolipids from *Gymnodinium* species. *Phytochemistry* 47:783–787.
- Prince, E. K., Lettieri, L., McCurdy, K. J. & Kubanek, J. 2006. Fitness consequences for copepods feeding on a red tide dinoflagellate: deciphering the effects of nutritional value, toxicity, and feeding behavior. *Oecologia* 147:479–488.
- Quy, O. M., Fotedar, R. & Thy, H. T. T. 2018. Extension of ro-

- tifer (*Brachionus plicatilis*) inclusions in the larval diets of mud crab, *Sylla paramamosain* (Estampador, 1949): effects on survival, growth, metamorphosis and development time. *Mod. Appl. Sci.* 12:65–74.
- Ronquist, F., Teslenko, M., van Der Mark, P., Ayres, D. L., Darling, A., Höhna, S., Larget, B., Liu, L., Suchard, M. A. & Huelsenbeck, J. P. 2012. MrBayes 3.2: efficient Bayesian phylogenetic inference and model choice across a large model space. *Syst. Biol.* 61:539–542.
- Rossini, G. P. 2014. *Toxins and biologically active compounds from microalgae*. CRC Press, Boca Raton, FL, 542 pp.
- Sakakura, Y. 2017. Application of rotifers for larval rearing of marine fishes cultivated under various conditions. In Hagiwara, A. & Yoshinaga, T. (Eds.) *Rotifers: Aquaculture, Ecology, Gerontology, and Ecotoxicology*. Springer Singapore, Singapore, pp. 63–73.
- Saldarriaga, J. F., Taylor, F. J. R., Keeling, P. J. & Cavalier-Smith, T. 2001. Dinoflagellate nuclear SSU rRNA phylogeny suggests multiple plastid losses and replacements. *J. Mol. Evol.* 53:204–213.
- Scholin, C. A., Herzog, M., Sogin, M. & Anderson, D. M. 1994. Identification of group- and strain-specific genetic markers for globally distributed *Alexandrium* (dinophyceae). II. Sequence analysis of a fragment of the LSU rRNA gene. *J. Phycol.* 30:999–1011.
- Sekida, S., Okuda, K., Katsumata, K. & Horiguchi, T. 2003. A novel type of body scale found in two strains of *Amphidinium* species (Dinophyceae). *Phycologia* 42:661–666.
- Sorgeloos, P., Dhert, P. & Candreva, P. 2001. Use of the brine shrimp, *Artemia* spp., in marine fish larviculture. *Aquaculture* 200:147–159.
- Sparmann, S. F., Leander, B. S. & Hoppenrath, M. 2008. Comparative morphology and molecular phylogeny of *Apicoporus* n. gen.: a new genus of marine benthic dinoflagellates formerly classified within *Amphidinium*. *Protist* 159:383–399.
- Spurr, A. R. 1969. A low-viscosity epoxy resin embedding medium for electron microscopy. *J. Ultrastruct. Res.* 26:31–43.
- Stamatakis, A. 2006. RAxML-VI-HPC: maximum likelihood-based phylogenetic analyses with thousands of taxa and mixed models. *Bioinformatics* 22:2688–2690.
- Stern, R. F., Andersen, R. A., Jameson, I., Küpper, F. C., Cofroth, M. -A., Vaulot, D., Le Gall, F., Véron, B., Brand, J. J., Skelton, H., Kasai, F., Lilly, E. L. & Keeling, P. J. 2012. Evaluating the ribosomal internal transcribed spacer (ITS) as a candidate dinoflagellate barcode marker. *PLoS ONE* 7:e42780.
- Sterzelecki, F. C., dos Santos Cipriano, F., Vasconcelos, V. R., Sugai, J. K., Mattos, J. J., Derner, R. B., Magnotti, C. F., Lopes, R. G. & Cerqueira, V. R. 2021. Minimum rotifer density for best growth, survival and nutritional status of Brazilian sardine larvae, *Sardinella brasiliensis*. *Aquaculture* 534:736264.
- Sun, Y., Hou, X., Xue, X., Zhang, L., Zhu, X., Huang, Y., Chen, Y. & Yang, Z. 2017. Trade-off between reproduction and lifespan of the rotifer *Brachionus plicatilis* under different food conditions. *Sci. Rep.* 7:15370.
- Takano, Y. & Horiguchi, T. 2004. Surface ultrastructure and molecular phylogenetics of four unarmored heterotrophic dinoflagellates, including the type species of the genus *Gyrodinium* (Dinophyceae). *Phycol. Res.* 52:107–116.
- Tamura, M., Takano, Y. & Horiguchi, T. 2009. Discovery of a novel type of body scale in the marine dinoflagellate, *Amphidinium cupulatisquama* sp. nov. (Dinophyceae). *Phycol. Res.* 57:304–312.
- Tester, P. A., Litaker, R. W. & Berdalet, E. 2020. Climate change and harmful benthic microalgae. *Harmful Algae* 91:101655.
- Turner, J. T. & Tester, P. A. 1997. Toxic marine phytoplankton, zooplankton grazers, and pelagic food webs. *Limnol. Oceanogr.* 42:1203–1213.
- Wellkamp, M., García-Camacho, F., Durán-Riveroll, L. M., Tebben, J., Tillmann, U. & Krock, B. 2020. LC-MS/MS method development for the discovery and identification of amphidinols produced by *Amphidinium*. *Mar. Drugs* 18:497.
- Wu, J., Long, L., Song, Y., Zhang, S., Li, Q., Huang, J. & Xiao, Z. 2005. A new unsaturated glycerolipid from a cultured marine dinoflagellate *Amphidinium carterae*. *Chem. Pharm. Bull.* 53:330–332.
- Yan, T., Wang, Y., Wang, L., Chen, Y., Han, G. & Zhou, M. 2009. Application of rotifer *Brachionus plicatilis* in detecting the toxicity of harmful algae. *Chin. J. Oceanol. Limnol.* 27:376–382.
- Yong, H. L., Mustapa, N. I., Lee, L. K., Lim, Z. F., Tan, T. H., Usup, G., Gu, H., Litaker, R. W., Tester, P. A., Lim, P. T. & Leaw, C. P. 2018. Habitat complexity affects benthic harmful dinoflagellate assemblages in the fringing reef of Rawa Island, Malaysia. *Harmful Algae* 78:56–68.
- Yoshida, T., Nakai, R., Seto, H., Wang, M. -K., Iwataki, M. & Hiroishi, S. 2003. Sequence analysis of 5.8S rDNA and the internal transcribed spacer region in dinoflagellate *Heterocapsa* species (Dinophyceae) and development of selective PCR primers for the bivalve killer *Heterocapsa circularisquama*. *Microbes Environ.* 18:216–222.
- Zhang, H. 2015. Diversity, phylogeny and distribution of benthic dinoflagellates in Hainan Island, China. Ph.D. dissertation, Jinan University, Guangzhou.